nature materials

LETTERS

PUBLISHED ONLINE: 1 JUNE 2014 | DOI: 10.1038/NMAT3985

Ultrahigh interlayer friction in multiwalled boron nitride nanotubes

A. Niguès[1], A. Siria[1]*, P. Vincent[1], P. Poncharal[1] and L. Bocquet[1,2]

Friction at the nanoscale has revealed a wealth of behaviours that depart strongly from the long-standing macroscopic laws of Amontons–Coulomb[1,2]. Here, by using a 'Christmas cracker'-type of system in which a multiwalled nanotube is torn apart between a quartz-tuning-fork-based atomic force microscope (TF–AFM) and a nanomanipulator, we compare the mechanical response of multiwalled carbon nanotubes (CNTs) and multiwalled boron nitride nanotubes (BNNTs) during the fracture and telescopic sliding of the layers. We found that the interlayer friction for insulating BNNTs results in ultrahigh viscous-like dissipation that is proportional to the contact area, whereas for the semimetallic CNTs the sliding friction vanishes within experimental uncertainty. We ascribe this difference to the ionic character of the BN, which allows charge localization. The interlayer viscous friction of BNNTs suggests that BNNT membranes could serve as extremely efficient shock-absorbing surfaces.

Considerable progress has been made recently in the understanding of the atomic origin of friction thanks to the development of powerful nanoscale tools[1–9]. Whereas macroscopic friction properties exhibit a relatively weak variation for various sliding materials, the dissipation at the atomic scale depends crucially on the detailed atomic nature of the constituents of the surfaces. A number of recent experiments and advanced computational work have allowed the disentanglement of the various contributions to the friction process, including the phononic, electronic and van der Waals contributions, as well as the role of commensurability or adsorbates[1,3,4,10–13]. In this quest, graphitic systems and carbon nanotubes constitute unique systems to gain an understanding of friction at the molecular level[8,14–16]. In particular, multiwalled nanotubes (MWNTs) exhibit concentric crystalline layers, which can *de facto* slide against each other with pure one-dimensional directional motion. The pioneering work of Zettl *et al.* demonstrated that CNTs exhibit an ultralow interlayer friction[14,15], in line with the measured superlubricity of graphite[4]. However, beyond the geometrical commensuration effects between graphitic layers, the origin of the ultralow friction raises many fundamental questions. It would, therefore, be highly desirable to make a detailed comparison with alternative materials of similar geometry to gain an insight into the mechanisms at work.

Here we report a systematic comparative study of the interlayer mechanics of carbon and boron nitride multiwalled nanotubes. Surprisingly, BNNTs exhibit a very similar crystallographic structure to carbon nanotubes, but radically different electronic properties[17]: C-MWNTs are conductors whereas BN-MWNTs are high-gap insulators. This makes BNNTs a promising material in the domain of nanomechanics[17], as well as in the context of energy harvesting[18].

To study the tribological response of stretched MWNTs we have performed tensile load experiments on individual nanostructures using an in-house-built nanomanipulator coupled to a quartz tuning fork (TF) as force sensor, inside a scanning electron microscope (FEI-Nova nanoSEM), see Fig. 1. Although quartz tuning forks have been widely implemented in the context of scanning probe microscopy[19,20], their use for quantitative force measurements is much more recent[21,22]. The advantages of this device are twofold: first, an ultrahigh stiffness of $k \approx 40\,\mathrm{kN\,m^{-1}}$, which prevents mechanical instability during the outer shell fracture; second, very low intrinsic dissipation—as characterized by high quality factors of up to $Q \approx 100{,}000$ in vacuum—and a very low oscillation amplitude (≈0.2–1 nm). These make it an ideal tool for friction studies.

The set-up is assembled in the form of a 'Christmas cracker'. Initially, a MWNT—carbon or boron nitride—is glued on an etched tungsten tip, whereas a second tungsten tip is glued on one arm of the tuning fork. Gluing is achieved by local cracking of naphtalene using a local electron-beam-induced deposition (EBID) process[18]. The tip–nanotube is mounted on a mobile stage of *xyz* step motors (Attocube N51xyz) with nanometer precision. Then the two parts of the set-up are brought together by nanomanipulation in the SEM and assembled by EBID.

The nanostructures are stretched by retracting the mobile tip on the manipulator. During the displacement both the position of the mobile tip and the electro-mechanical response of the tuning fork are simultaneously recorded. The relative motion of the mobile and fixed tips is controlled by the command voltage to the piezo element.

For a given separation between the fork and the nanomanipulation stage (x), the mechanical properties of the MWNT are measured quantitatively by analysing the frequency response of the tuning fork coupled to the MWNT device under a given oscillation amplitude. The system behaves as a mass–spring resonator[19], whose resonance frequency is shifted under the position-dependent force $F(x)$ applied by the MWNT on the tuning fork. It can be easily shown that the resonance frequency shift δf is related to the force gradient ∇F according to[19]

$$\delta f = -\nabla F \frac{f_0}{2k_{\mathrm{TF}}} \tag{1}$$

where f_0 is the bare resonance frequency and k_{TF} is the tuning fork spring constant.

Furthermore, the dissipation can be extracted from a measurement of the quality factor of the resonance width (Fig. 1c). In vacuum and under our experimental conditions, the tuning-fork resolution for the frequency shift is 10 mHz, corresponding to

[1]Institut Lumière Matière, UMR5306 Université Lyon 1-CNRS, 69622 Villeurbanne cedex, France, [2]Department of Civil and Environmental Engineering, Massachusetts Institute of Technology, UMI 3466 CNRS-MIT, Cambridge, Massachusetts 02139, USA. *e-mail: alessandro.siria@univ-lyon1.fr

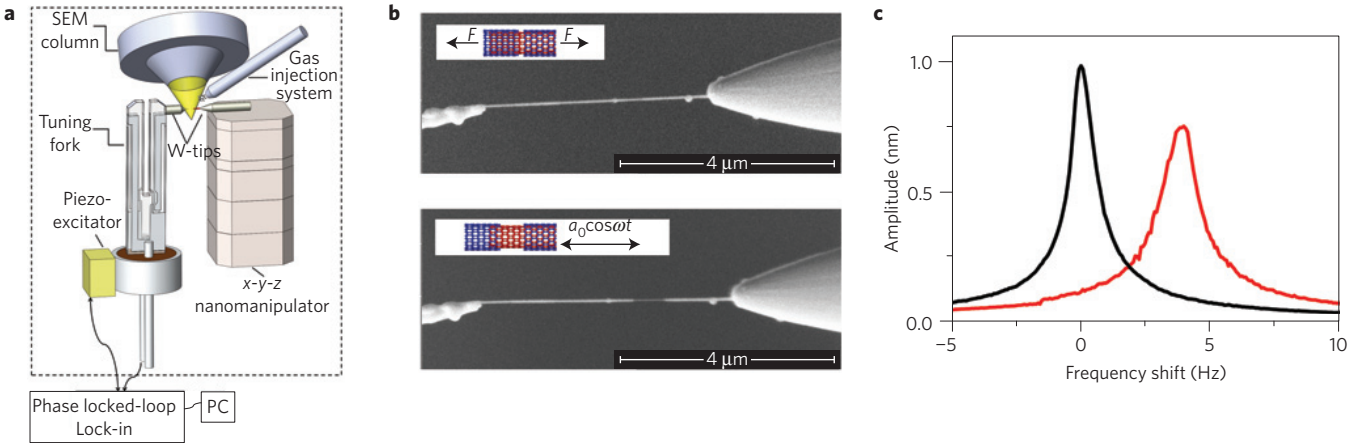

Figure 1 | Multiwalled nanotube Christmas-cracker experimental set-up. a, Schematic drawing of the experiments, showing a multiwalled nanotube assembled to a tuning-fork on one side, and to a nanomanipulator on the other side. A piezo system excites the oscillator at the resonance frequency (≈32 kHz); a lock-in and a phase-locked loop maintain both the amplitude and the phase constant between the tuning fork and the excitator. **b**, SEM images of a carbon nanotube glued to each tungsten tip during the tensile experiments. Nanotube length = 5.5 μm, external diameter 60 nm, sliding tube diameter 25 nm. **c**, Amplitude resonance curves for both free and interacting tuning forks. The black curve represents the free resonator oscillating in vacuum with a quality factor $Q = 45{,}000$. The red curve represents the tuning-fork response during telescopic intershell sliding with a quality factor $Q = 18{,}000$.

14 mN m^{-1} resolution for the stiffness measurement. A minimal change of ∼2,000 in the quality factor can be measured, corresponding to a resolution on the dissipation part of the force in the 20 pN range. As discussed below, benchmark tests on SiC nanowire and nanotubes allow one to check that the carbon gluing via EBID is extremely stiff and does not contribute to the measured stiffness of the tube or to its dissipation.

Before exploring the mechanical response of CNTs and BNNTs, we first performed benchmark experiments on a silicon carbide nanowire (SiC-NW), see Fig. 2a. Starting from a relaxed configuration, the nanowire is put under tension by continuously displacing the nanomanipulation stage by a distance x along its length. For each position x the frequency-dependent response of the nanowire is recorded. A positive frequency shift is measured, typically in the range 10–50 Hz, first increasing with x and then reaching a plateau after a displacement of $x \approx 50$ nm. As the frequency shift is proportional to the spatial gradient, $\nabla_x F$, of the restoring force, this plateau corresponds to an elastic response of the nanowire, with constant axis stiffness $k_{NW} = 140$ N m^{-1} as deduced from equation (1). This value is related to the Young's modulus according to $k_{NW} = Y\mathcal{A}/L$, where $\mathcal{A}$ is the cross-sectional area and L the length of the NW. In our experimental configuration with $k_{NW} = 140$ N m^{-1}, $L = 50$ μm and NW radius $R = 75$ nm, one gets $Y \simeq 400$ GPa, in good agreement with previous experimental data for nanowires of SiC (ref. 23).

Pulling further leads to fracture of the SiC-NW, at ≈ 3.2% elongation (see Fig. 2a), as signalled by the abrupt drop of the frequency shift towards zero. The results of this benchmark experiment confirm that the force-measurement set-up allows quantitative measurements of the mechanical properties of nanoscale materials.

We now turn to the case of carbon and boron nitride nanotubes, which are the main focus of the present study. The CNTs were fabricated by arc discharge and characterized by transmission electron microscopy, showing a very high structural quality, as already checked in a previous study[24]; BNNTs were synthesized by chemical vapour deposition and characterized by transmission electron microscopy and electron energy loss spectroscopy, also showing a very high structural quality[25] (see Supplementary Methods for transmission electron microscope (TEM) characterization of nanotubes). The study has been performed on ten different nanotubes of each type, showing similar results. In the following, we show results for BNNTs and CNTs presenting comparable interacting interlayer surfaces.

As shown in Fig. 2b,c, the response for the stiffness of the multilayer CNTs and BNNTs is quite different from the previous SiC-NW. After an initial increase in the frequency shift, a first abrupt drop is observed (as indicated by the arrow) before any plateau is reached. From the frequency shift just before fracture, one can estimate only a lower bound for the elastic modulus of the CNTs and BNNTs, which is found to be of the order of hundreds of GPa, in agreement with expectations from the literature[17]. However, after the drop, the frequency shift—and hence the deduced stiffness—does not vanish after the fracture, but rather decreases gradually as the elongation increases. The decrease in the stiffness is roughly an affine function of the displacement. The first drop corresponds to a fracture occurring in the outer layer of the MWNT, and the subsequent phase corresponds to the telescopic sliding of the outer layer over the inner layers (see sketch in Fig. 2b,c). The fact that the stiffness does not vanish after the first fracture is by no means obvious and indicates a remaining elastic interaction between the various layers under shear. As shown in Fig. 2d, the stiffness k measured for the BNNT is considerably larger than for the CNT, suggesting a much stronger molecular interaction between BNNT layers than between CNT layers, in agreement with previous torsion measurements[27].

To go further, the interaction between atoms in the sliding shell can be described as a spring, whose stiffness $k_{int,i}$ is attributed to the direct interaction between atoms of the interacting layers (see sketch in Fig. 3d). In this approximation the frequency shift measured by the tuning fork is given by:

$$\delta f \propto -\frac{\partial F}{\partial x} \approx N\, k_{int,i} = \rho \mathcal{A}\, k_{int,i} \qquad (2)$$

where N is the number of interacting atoms, ρ the atom surface density and $\mathcal{A}$ the contact area. This expression suggests a linear dependence of the NT stiffness on the interacting surface, as experimentally observed in Fig. 2d.

We now focus on the dissipation and friction occurring during the interlayer sliding of MW-CNTs and MW-BNNTs. To this end,

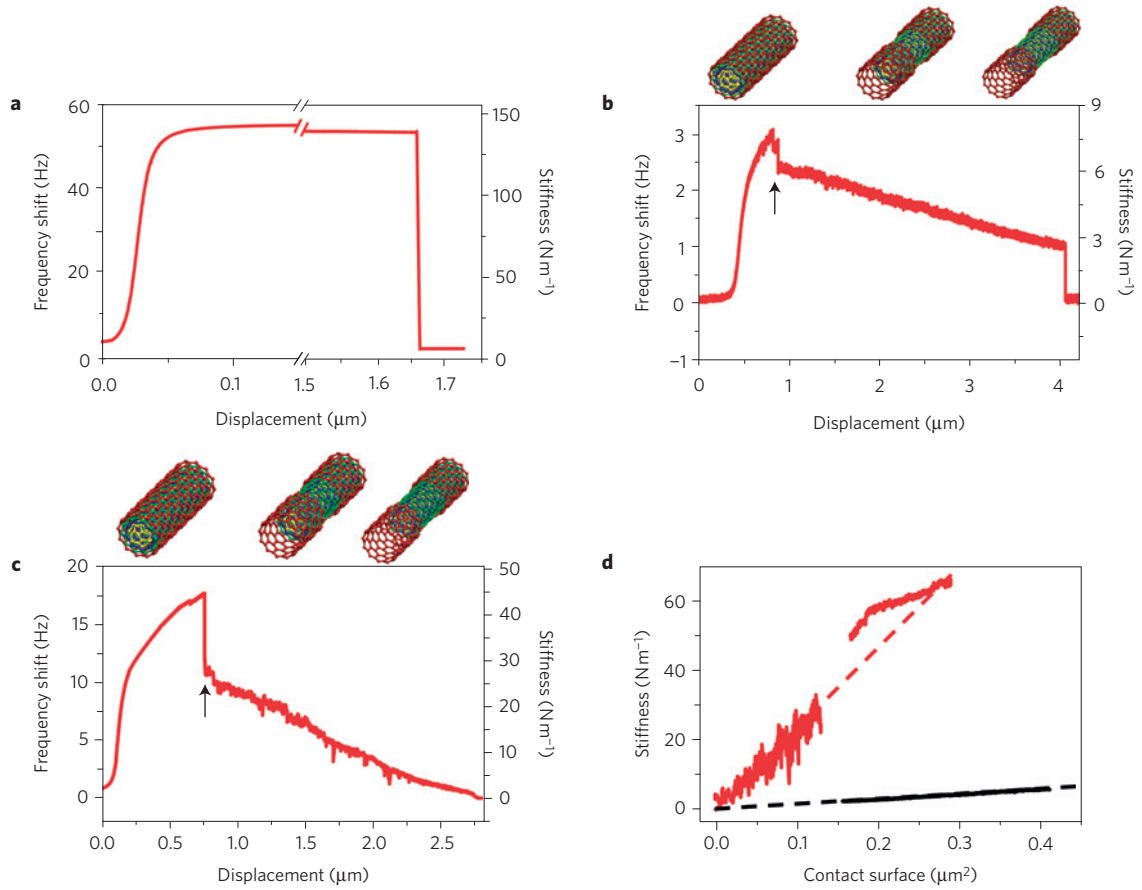

Figure 2 | Frequency shift measured by the tuning fork versus the displacement of the piezoscanner during complete tensile load experiments. **a**, SiC-NW with length $L=50\,\mu m$ and radius $R=75$ nm. **b**, Multiwalled CNT with $L_0=4.5\,\mu m$ and outer radius $R=20$ nm. The arrow indicates the occurrence of the first fracture for the outer layers of the nanotube. The final jump to zero corresponds to complete uncoiling of the nanotube, starting before the complete sliding of the nanotube. **c**, Multiwalled BNNT with length $L_0=3\,\mu m$ and outer radius $R=40$ nm. The arrow denotes the occurrence of the first fracture for the outer layers of the nanotube. **d**, Intershell stiffness of the nanotubes as a function of the intershell surface interaction area. Red and black curves are for the BNNT and CNT, respectively. The dashed lines are linear fits, $k=C\times\mathcal{A}$, with $C=2.4\times10^{14}$ N m^{-3} for the BNNT (red dashed line) and $C=1.5\times10^{13}$ N m^{-3} for the CNT (black dashed line).

we measure the full mechanical response function of the tuning fork, as shown in Fig. 1c. A first key observation is that, for all conditions explored, the resonance curve is perfectly fitted by a resonance of damped-harmonic-oscillator type

$$a(\omega)=a_0\cdot\frac{\omega_R/\omega}{\sqrt{1+Q^2\left(\omega/\omega_R-\omega_R/\omega\right)^2}} \qquad (3)$$

with $\omega_R=2\pi f_R$, f_R the resonance frequency, and Q the quality factor (see Fig. 3a for the case of a given MW-BNNT for various positions x). This resonance corresponds to the response of a damped harmonic oscillator, demonstrating that the friction during the interlayer sliding is of the viscous type, with a frictional force proportional to the interlayer velocity as $F_f=-\gamma\times V$, with γ being the friction coefficient. As can be expected for nanoscale dissipation, the friction is not of the Coulomb–Amontons type[3]. Going deeper into the quantitative analysis, the dissipation is extracted from the quality factor Q of the resonance curve. In practice, we maintain the amplitude of oscillation of the tuning fork constant at a value $a_0=1$ nm via a feedback loop, and measure the required excitation voltage V_{ex} (associated with the excitation forcing). For an externally excited damped oscillator, it is easy to show that the oscillation amplitude a_R at resonance is proportional to the excitation voltage V_{ex} via the relation $a_R\propto Q/k_{TF}\times V_{ex}$, with a proportionality constant which is only a function of the set-up. Then, for a given configuration (position x of the MW-CNT or MW-BNNT) and amplitude ($a_R=a_0$), one obtains a direct relation between the parameters with and without the nanotube, as $Q_{int}/Q_0=V_0/V_{int}$, where the index 0 denotes the free tuning fork, and 'int' denotes the parameters measured with a nanotube. The dissipative force computed at the resonance frequency is deduced as[19]

$$F_D(\omega_R)=\frac{k_{TF}a_0}{\sqrt{3}}\left(\frac{1}{Q_{int}}-\frac{1}{Q_0}\right) \qquad (4)$$

and the viscous-like friction coefficient, γ, defined above is deduced as $\gamma=F_D/v$, where $v=\omega_R a_0$ is the velocity at the resonance frequency. Note that, as a supplementary check, we have varied the relative sliding velocity by increasing the oscillation amplitude of the tuning fork (up to 4 nm), yielding similar results (see Fig. 3b). In Fig. 3c we plot the resulting dissipation force, F_D, and friction coefficient γ for both a MW-CNT and a MW-BNNT versus the contact area between the sliding layers, $\mathcal{A}=2\pi R\times L$, where L is the contact length and R the corresponding intershell radius obtained by post-mortem observation in a TEM (Fig. 3d). Note that the contact length is obtained from the displacement of the tuning fork with respect to the mobile tip.

A first striking observation is the huge difference between the dissipation measured in these two systems. The dissipation force

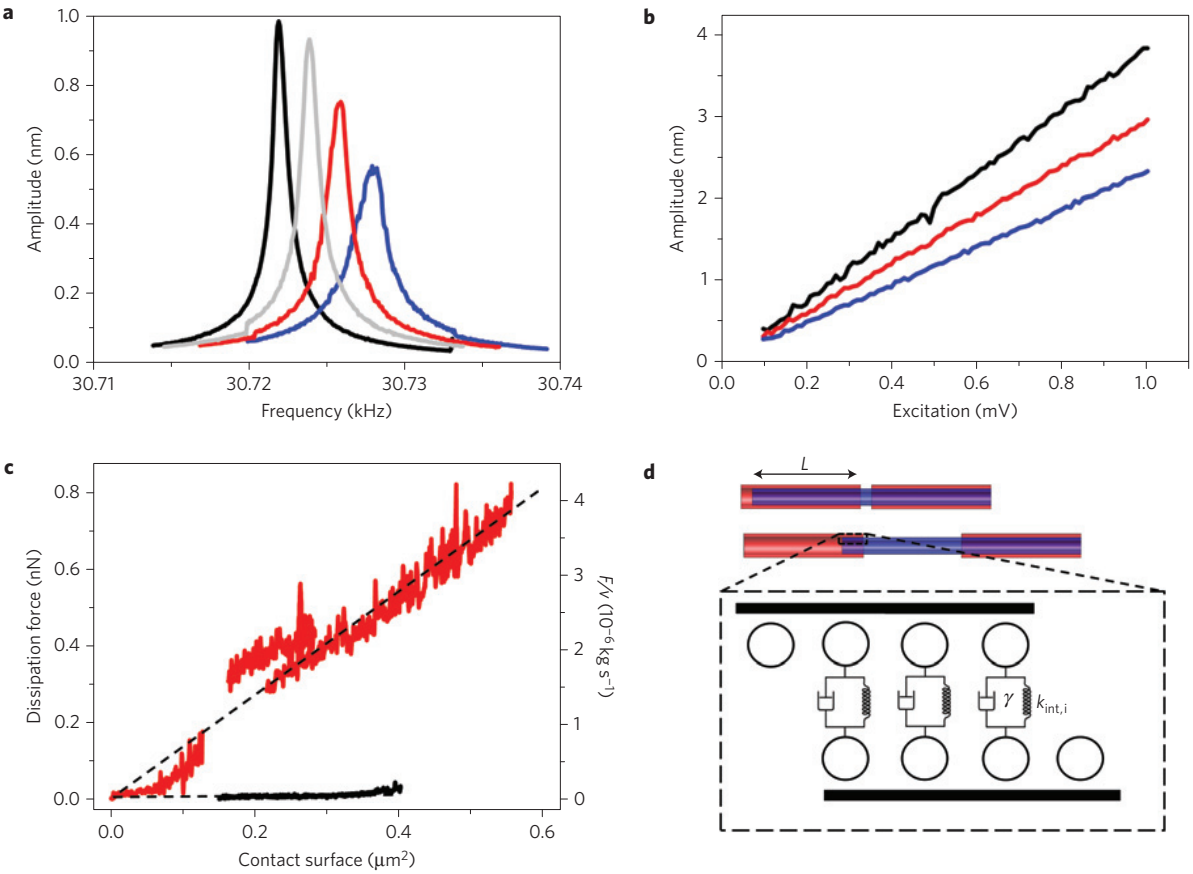

Figure 3 | Interlayer friction in multiwalled nanotubes. a, Resonance curves measured for various contact lengths L between the sliding layers. Data are obtained for the same BNNT as presented in Fig. 2c. The contact length L decreases (from blue to black); Q factors are obtained by fitting to equation (3), leading to $Q=18\times10^3$, 26×10^3, 33.5×10^3 and 41×10^3 (from blue to black). **b**, Amplitude of the tuning fork versus excitation voltage as the contact length L decreases (from blue to black). The quality factor $Q_{int}=V_0/V_{int}\times Q_0$, where the index 0 denotes the free tuning fork and 'int' denotes the parameters measured with a nanotube (see text). **c**, Dissipation force and friction coefficient versus the interlayer contact area: concentric BNNTs (red), concentric CNTs (black). Nanotube characteristics: BNNT1 $L=3\,\mu$m, diameter $D=65$ nm; BNNT2 $L=7\,\mu$m, diameter $D=60$ nm; CNT $L=4.5\,\mu$m, outer diameter $D=30$ nm. **d**, Schematic for intershell friction in nanotubes: the interatomic interaction is represented by a viscoelastic dashpot model with stiffness $k_{int,i}$ and damping γ.

and friction coefficients are extremely weak for MW-CNT sliding layers with intershell radius $R=12$ nm. This is in agreement with previous reports in the literature, where vanishing friction has been observed in microscale nanotubes under vacuum condition[14,15] and in centimetre long double-wall CNTs in ambient conditions[16]. In all cases, the structural properties of the system are key to the observed superlubricity.

In sharp contrast, the frictional force is orders of magnitude larger for interlayer sliding inside the MW-BNNT. Moreover the friction coefficient γ is measured to be proportional to the contact area, $\gamma\propto\mathcal{A}$, such that in combination $F_D=-\lambda\times\mathcal{A}\times v$, with λ the friction coefficient. Note that Fig. 3b shows collapsed data obtained for various BNNTs. Experiments have been performed with intershell radii $R_1=10$ nm, $R_2=25$ nm and $R_3=25$ nm, and different lengths. We detected no dependence of the friction coefficient λ on the radius within the range of analysis.

Altogether, our results demonstrate that MW-CNTs and MW-BNNTs—although exhibiting very similar crystallographic and structural properties—differ radically in terms of their frictional properties. One key difference between the systems is the ionic character of BN, which may increase the interlayer electrostatic interactions, in contrast with carbon, which is associated with covalent, charge-neutral interactions. Thus, to gain an insight into this puzzling observation, we first investigated in more detail the origin of the frictional drag in the present system. In general, one may separate the frictional drag into an electronic and a phononic contribution—and theories describing these contributions have been developed in the literature[2,3]. However, the electronic contribution to the frictional drag should be absent for the strongly insulating BNNT, and present only for the semi-metallic CNT. This shows, therefore, that the electronic contributions in CNTs are negligible and cannot be the origin of the observed behaviour. On the other hand, the phononic contribution is expected to be proportional to the interaction area $\mathcal{A}$ and to the square of the energy corrugation, U_0 (or barrier height of the interlayer potential), as[3]

$$\gamma_{ph}=a\,\mathcal{A}\times U_0^2 \qquad (5)$$

with a being a constant dependent on temperature and structural parameters, which are similar for CNTs and BNNTs. This result can be understood in simple terms. The friction coefficient should obey the fluctuation–dissipation theorem, so that $\gamma=1/k_BT\int_0^\infty\langle F(t)\times F(0)\rangle dt$, with $F(t)$ the lateral interlayer fluctuating force, k_B the Boltzmann constant, T the temperature and t time. As $F\propto U_0$, one therefore expects that $\gamma\propto U_0^2$. Now, in contrast to CNTs, BNNTs are ionic in nature, with a partial charge separation $\delta q\sim0.3$–$0.4e$ on the B and N atoms[17]. This shows that the barrier height U_0 for the BNNTs should be affected by electrostatic interactions, with $U_0\sim\delta q^2/4\pi\epsilon d$ (with $d\sim3$ Å being the interlayer

spacing and ϵ the dielectric permittivity), whereas only dispersive interaction forces apply for the CNTs. This difference is in agreement with the strong difference in the measured interlayer stiffness between CNTs and BNNTs, which is typically expected to scale like U_0. Scaling as U_0^2, the frictional drag is expected to be even more pronounced, as indeed measured experimentally. One actually expects that $\gamma_{BNNT}/\gamma_{CNT} \sim (k_{BNNT}/k_{CNT})^2$, so that the two drags are expected to differ by more than two orders of magnitude as $k_{BNNT}/k_{CNT} \approx 16$, see Fig. 2d. This is in good agreement with our observations in Fig. 3c. As an alternative and complementary mechanism, strong wall–wall interactions due to the ionic character of BN bonds were proposed to induce some structural reorganization of the BNNT layers, with some possible faceting[26], resulting in interlayer locking and high stiffness[27]. We expect that this behaviour should increase the longitudinal friction between layers for BNNTs. Disentangling the various mechanisms would require a systematic theoretical exploration to obtain quantitative estimates of the various contributions to friction and dissipation remaining, which we leave for future work.

Furthermore, it is interesting to compare our findings with those in ref. 28, which shows that friction between an AFM tip and a nanotube on a substrate in air is larger in the case of BNNTs than for arc-discharge CNTs. Moreover, an anisotropy in the transverse and longitudinal friction in BNNTs is reported, which the authors ascribe to interactions with the substrate. Here, by working in vacuum with tensile-load experiments on suspended nanotubes, we also show that the intershell friction in BNNTs is several orders of magnitude larger than in arc-discharge CNTs. We conjecture that a similar phenomenon may also be at the origin of the findings of ref. 28.

Finally, it is interesting to note that the drag coefficient for the BNNT dissipation is of considerable magnitude, as can be realized by comparing it against the frictional drag of alternative materials. Defining a damping term per unit surface as $\lambda = -F_D/(\mathcal{A}\, v)$, one gets for the BNNT a value of $\lambda \simeq 6.7 \times 10^6\,\mathrm{kg\,m^{-2}\,s^{-1}}$. Data for the coefficient λ for alternative materials are available in the quartz crystal microbalance literature[3], in terms of the slip time of adsorbed layers over various surfaces. For solid monolayers and slip times which are typically in the nanosecond range, the corresponding values for λ are roughly in the range 10^2–$10^4\,\mathrm{kg\,m^{-2}\,s^{-1}}$ depending on the materials considered[3], which is at least two orders of magnitude smaller than the frictional drag measured for the BN material. From an alternative perspective, one may consider how much dissipation could be achieved using a macrosopic membrane made of a collection of such vertical BNNTs, say $1\,\mathrm{cm^2}$ in size, that are able to undergo telescopic sliding. Assuming a density of 10^{10} BNNTs per $\mathrm{cm^2}$ and a maximum surface change of $0.5\,\mu\mathrm{m^2}$ per BNNT, as in the present experiment, one gets a total frictional drag of $\gamma_{tot} \approx 4 \times 10^4\,\mathrm{kg\,s^{-1}}$. To achieve this value with a classical fluid dashpot with similar centimetric size D, one would typically need a fluid with an equivalent viscosity $\eta \equiv \gamma/(3\pi D) \sim 10^5\,\mathrm{Pa\,s}$—that is, $\approx 10^8$ times the viscosity of water. These estimates indicate the extremely high efficiency of membranes made of such multilayer BNNTs as shock-absorbing surfaces.

Methods

Nanotubes are prepared by gluing them individually on an electrochemically etched tungsten tip. BNNTs are first culled under optical observation and glued with carbon tape; bonding is then reinforced before manipulation by EBID. CNTs are directly selected under SEM observation and glued by EBID. An etched tungsten tip is glued with conductive epoxy on one arm of the TF, as used in scanning probe microscopy. On the sample holder of the SEM, the TF and the prepared nanotubes are placed face-to-face on a dedicated nanomanipulation station. The TF is placed on the motionless part, whereas the tip–nanotube is mounted on part move by the *xyz* stepper motors. During the displacement (speed $25\,\mathrm{nm\,s^{-1}}$), both the position of the mobile tip, recorded through the voltage applied, and the signals provided from the TF, usually excited by means of piezoelectric dithering, allowing a natural mechanical excitation, are simultaneously recorded.

Nanotubes have been characterized by transmission electron microscopy, with a TopCon microscope operated at 120 kV and 200 kV. Arc-discharge CNTs and chemical vapour deposition BNNTs used during the experiments present a very high structural purity with no evident defects in a spatial region in the micrometre range, comparable to the telescopic length of the experiments . No clear difference is presented between CNTs and BNNTs.

After the tensile load experiment, nanotubes were imaged with a TEM working at 200 kV to obtain the intershell diameter. Only nanotubes that have been glued on the tungsten wire can be imaged, owing to the dimensions of the tuning fork and lack of room for access inside the microscope column.

Received 18 December 2013; accepted 15 April 2014; published online 1 June 2014

References

1. Vanossi, A., Manini, N., Urbakh, M., Zapperi, S. & Tosatti, E. Modeling friction: From nanoscale to mesoscale. *Rev. Mod. Phys.* **85,** 529 (2013).
2. Persson, B. N. J. *Sliding Friction — Physical Principle and Applications* 2nd edn (Springer, 2000).
3. Krim, J. Friction and energy dissipation mechanisms in adsorbed molecules and molecularly thin films. *Adv. Phys.* **61,** 155–323 (2012).
4. Dienwiebel, M. *et al.* Superlubricity of graphite. *Phys. Rev. Lett.* **92,** 126101 (2004).
5. Urbakh, M. & Meyer, E. The renaissance of friction. *Nature Mater.* **9,** 8–10 (2010).
6. Socoliuc, A. *et al.* Atomic-scale control of friction by actuation of nanometer-sized contacts. *Science* **313,** 207–210 (2006).
7. Lee, C. *et al.* Frictional characteristics of atomically thin sheets. *Science* **328,** 76–80 (2010).
8. Lucas, M. *et al.* Hindered rolling and friction anisotropy in supported nanotubes. *Nature Mater.* **87,** 876–881 (2009).
9. Jacobs, T. D. B. & Carpick, R. W. Nanoscale wear as a stress-assisted chemical reaction. *Nature Nanotech.* **8,** 108–112 (2013).
10. Kisiel, M. *et al.* Suppression of electronic friction on Nb films in the superconducting state. *Nature Mater.* **10,** 119–122 (2011).
11. Ogletree, D. F., Park, J. Y., Salmeron, M. & Thiel, P. A. Electronic control of friction in silicon pn junctions. *Science* **313,** 186 (2006).
12. Gostman, B. Tribology: sliding on vacuum. *Nature Mater.* **10,** 87–88 (2011).
13. Siria, A. *et al.* Electron fluctuation induced resonance broadening in nano electromechanical systems: The origin of shear force in vacuum. *Nano Lett.* **12,** 3551–3556 (2012).
14. Cumings, J. & Zettl, A. Low-friction nanoscale linear bearing realized from multiwall nanotubes. *Science* **289,** 602–604 (2000).
15. Kis, A. Jensen, K. Aloni, S. Mickelson & W. Zettl, A. Interlayer forces and ultralow sliding friction in multiwalled carbon nanotubes. *Phys. Rev. Lett.* **97,** 025501 (2006).
16. Zhang, R. *et al.* Superlubricity in centimetres-long double-walled carbon nanotubes under ambient conditions. *Nature Nanotech.* **8,** 912–916 (2013).
17. Arenal, R., Blase, X. & Loiseau, A. Boron-nitride and boron-carbonitride nanotubes: synthesis, characterization and theory. *Adv. Phys.* **59,** 101–179 (2010).
18. Siria, A. *et al.* Giant osmotic energy conversion in a single transmembrane boron nitride nanotube. *Nature* **494,** 455–458 (2013).
19. Karrai, K. & Grober, R. D. Piezoelectric tip–sample distance control for near field optical microscopes. *Appl. Phys. Lett.* **66,** 1842 (1995).
20. Giessibl, F. J. High-speed froce sensor for force microscopy and profilometry utilizing a quartz tuning fork. *Appl. Phys. Lett.* **73,** 3956 (1998).
21. Labardi, M. & Allegrini, M. Non-contact friction force microscopy based on quartz tuning fork sensors. *Appl. Phys. Lett.* **89,** 174104 (2006).
22. Rodrigues, M. *et al.* Probing the elastic properties of individual nanostructures by combining *in-situ* atomic force micrscopy and micro-X-ray diffraction. *Appl. Phys. Lett.* **94,** 23109 (2009).
23. Perisanu, S. *et al.* Mechanical properties of SiC nanowires determined by scanning electron and field emission microscopies. *Phys. Rev. B.* **77,** 165434 (2008).
24. Poncharal, P., Wang, Z. L., Ugarte, D. & de Heer, W. A. Electrostatic deflections and electromechanical resonances of carbon nanotubes. *Science* **283,** 1513–1516 (1999).
25. Bechelany, M. *et al.* Preparation of BN microtubes/nanotubes with unique chemical process. *J. Phys. Chem. C* **112,** 18325 (2008).

26. Celik-Aktas, A., Zuo, J-M., Stubbins, J. F., Tang, C. & Bando, Y. Double-helix structure in multiwall boron nitride nanotubes. *Acta Crystallogr.* **A61,** 533–541 (2005).
27. Garel, J. *et al.* Ultrahigh torsional stiffness and strength of boron nitride nanotubes. *Nano Lett.* **12,** 6347–6352 (2012).
28. Chui, H- C., Dogan, S., Volkmann, M., Klinke, C. & Riedo, E. Adhesion and size dependent friction anisotropy in boron nitride nanotubes. *Nanotechnology* **23,** 455706 (2012).

Acknowledgements

A.S. and L.B. thank M.L. Bocquet for many fruitful discussions on CNTs and BNNTs. P.P. and P.V. thank N. Blanchard for support in TEM imaging of the nanotubes. The authors acknowledge support of an ERC advanced grant, project *Micromegas*.

Author contributions

A.S. conceived the project. A.N. performed the experiments. A.N., A.S. and L.B. performed the data analysis. A.N. and A.S. conceived and realized the experimental set-up. P.P. and P.V. characterized the nanotubes. A.S. and L.B. wrote the article with inputs from A.N. and P.P. A.S. and L.B. supervised the project.

Additional information

Supplementary information is available in the online version of the paper. Reprints and permissions information is available online at www.nature.com/reprints. Correspondence and requests for materials should be addressed to A.S.

Competing financial interests

The authors declare no competing financial interests.